

ALES Shallow-Water Flow Solver with Non-Hydrostatic Pressure: Wave Applications

J. G. Zhou¹ and P. K. Stansby²

Abstract

A shallow-water flow solver with non-hydrostatic pressure in σ coordinates has been developed to include effects due to the moving grid, referred to as the ALES approach. The formulation is outlined for 2D vertical plane problems and tested against experimental data for wave flows over plane beds, bars and trenches. Agreement with experiment is generally good and the importance of non-hydrostatic pressure and moving-grid terms is demonstrated.

Introduction

Conventional shallow-water flow models based on hydrostatic pressure can provide accurate results for many engineering problems. However, the model will not be accurate for problems in which there is significant gradient of either bed topography or free surface. A recent study by Stansby and Zhou (1998) has shown that the influence of non-hydrostatic pressure on current flow over a trench with bottom slope greater than 1:5 can be significant. The solver developed for non-hydrostatic pressure applies also to wave flows. Accurate predictions of wave flows including viscous/turbulence effects are of importance in coastal and ocean engineering projects such as harbors, channel dredging, pipeline trenching and storm-surge barriers. In this paper, we present a shallow-water flow solver to predict waves over a plane bed, a trapezoidal trench and a bar and compare with experimental data. The model is based on the unsteady Reynolds-averaged Navier-Stokes equations in ALE (Hirt, 1970) description which is able to account for the moving mesh with non-hydrostatic pressure. The equations are solved in the σ coordinate system and the eddy viscosity is calculated using the standard $k - \epsilon$ model. The method is referred to as ALES. The computations are also compared with the model with hydrostatic pressure alone.

Flow Model

The unsteady Reynolds-averaged Navier-Stokes equations for incom-

¹Research Associate, Hydrodynamics Research Group, School of Engineering, The University of Manchester, Manchester M13 9PL, UK

²Professor, Hydrodynamics Research Group, School of Engineering, The University of Manchester, Manchester M13 9PL, UK

pressible flow in a 2-D vertical plane can be written with the ALE description for incompressible flow, with the Boussinesq assumption for the time-averaged Reynolds stress in σ coordinates as

$$\frac{\partial u}{\partial x} + \frac{\partial w}{\partial z} = 0 \tag{1}$$

$$\begin{aligned} \frac{\partial(hu)}{\partial t} + \frac{\partial(huu)}{\partial x} + \frac{\partial(\omega u)}{\partial \sigma} - w_g \frac{\partial u}{\partial \sigma} = & -gh \frac{\partial \eta}{\partial x} - \frac{h}{\rho} \frac{\partial \tilde{p}}{\partial x} \\ & + h \frac{\partial}{\partial x} \left(\nu_e \frac{\partial u}{\partial x} \right) + \frac{\partial}{\partial \sigma} \left(\frac{\nu_e}{h} \frac{\partial u}{\partial \sigma} \right) \end{aligned} \tag{2}$$

$$\begin{aligned} \frac{\partial(hw)}{\partial t} + \frac{\partial(huw)}{\partial x} + \frac{\partial(\omega w)}{\partial \sigma} - w_g \frac{\partial w}{\partial \sigma} = & -\frac{1}{\rho} \frac{\partial \tilde{p}}{\partial \sigma} \\ & + h \frac{\partial}{\partial x} \left(\nu_e \frac{\partial w}{\partial x} \right) + \frac{\partial}{\partial \sigma} \left(\frac{\nu_e}{h} \frac{\partial w}{\partial \sigma} \right) \end{aligned} \tag{3}$$

$$\frac{\partial \eta}{\partial t} + \frac{\partial}{\partial x} \int_{-1}^0 h u d\sigma = 0 \tag{4}$$

where x is the horizontal coordinate and σ the vertical dimensionless coordinate defined below; η is the water surface elevation above horizontal datum; h is water depth; u and w are the velocity components in the horizontal and vertical directions; $\omega = h d\sigma/dt$ (defined below); w_g is the grid velocity in the vertical direction; g is the gravitational acceleration; \tilde{p} is the non-hydrostatic pressure; ρ is the fluid density; ν_e is the eddy viscosity; where

$$\sigma = \frac{z - \eta}{h}, \quad \omega = w - u \left(\sigma \frac{\partial h}{\partial x} + \frac{\partial \eta}{\partial x} \right) - \left(\sigma \frac{\partial h}{\partial t} + \frac{\partial \eta}{\partial t} \right)$$

$\omega = 0$ when $\sigma = -1$ or $\sigma = 0$, corresponding to the bed and the free surface. The continuity equation (1) is not transformed into σ coordinates because the non-hydrostatic pressure is calculated in real space.

The eddy viscosity ν_e is defined by the standard $k - \epsilon$ equations (Rodi, 1993), which can be written in σ coordinates as

$$\begin{aligned} \frac{\partial(hk)}{\partial t} + \frac{\partial(huk)}{\partial x} + \frac{\partial(\omega k)}{\partial \sigma} - w_g \frac{\partial k}{\partial \sigma} = & h \frac{\partial}{\partial x} \left(\frac{\nu_e}{\sigma_k} \frac{\partial k}{\partial x} \right) \\ & + \frac{\partial}{\partial \sigma} \left(\frac{\nu_e}{h \sigma_k} \frac{\partial k}{\partial \sigma} \right) + hP - h\epsilon \end{aligned} \tag{5}$$

$$\begin{aligned} \frac{\partial(h\epsilon)}{\partial t} + \frac{\partial(hu\epsilon)}{\partial x} + \frac{\partial(\omega\epsilon)}{\partial\sigma} - w_g \frac{\partial\epsilon}{\partial\sigma} &= h \frac{\partial}{\partial x} \left(\frac{\nu_e}{\sigma_\epsilon} \frac{\partial\epsilon}{\partial x} \right) \\ &+ \frac{\partial}{\partial\sigma} \left(\frac{\nu_e}{h\sigma_\epsilon} \frac{\partial\epsilon}{\partial\sigma} \right) + hc_{1\epsilon} \frac{\epsilon}{k} P - hc_{2\epsilon} \frac{\epsilon^2}{k} \end{aligned} \quad (6)$$

Solution of the Equations

Spatial discretization is in finite-volume form on a staggered mesh following Stansby (1997). For a cell i, k the equations (2)-(4) can be discretized in time from time level n to $n+1$ with time step δt , as

$$\frac{\eta_i^{n+1} - \eta_i^n}{\delta t} + \frac{\partial}{\partial x} \int_{-1}^0 h_i^n [\theta u_{i,k}^{n+1} + (1-\theta)u_{i,k}^n] d\sigma = 0 \quad (7)$$

$$\begin{aligned} h_i^n \frac{u_{i,k}^{n+1} - u_{i,k}^n}{\delta t} + \frac{\partial(huu)_{i,k}^n}{\partial x} + \frac{\partial(\omega u)_{i,k}^n}{\partial\sigma} - w_{gi,k} \frac{\partial u_{i,k}^n}{\partial\sigma} &= \\ -gh_i^n \left[\theta \frac{\partial\eta_i^{n+1}}{\partial x} + (1-\theta) \frac{\partial\eta_i^n}{\partial x} \right] - \frac{h_i^n}{\rho} \frac{\partial\tilde{p}_{i,k}^n}{\partial x} + u_{i,k} \frac{\partial h_i}{\partial t} \\ + h_i^n \frac{\partial}{\partial x} \left(\nu_e \frac{\partial u_{i,k}^n}{\partial x} \right) + \frac{\partial}{\partial\sigma} \left(\frac{\nu_e}{h_i^n} \frac{\partial u_{i,k}^{n+1}}{\partial\sigma} \right) \end{aligned} \quad (8)$$

$$\begin{aligned} h_i^n \frac{w_{i,k}^{n+1} - w_{i,k}^n}{\delta t} + \frac{\partial(huw)_{i,k}^n}{\partial x} + \frac{\partial(\omega w)_{i,k}^n}{\partial\sigma} - w_{gi,k} \frac{\partial w_{i,k}^n}{\partial\sigma} &= \\ -\frac{1}{\rho} \frac{\partial\tilde{p}_{i,k}^n}{\partial\sigma} + w_{i,k} \frac{h_i^{n+1} - h_i^n}{\delta t} \\ + h_i^n \frac{\partial}{\partial x} \left(\nu_e \frac{\partial w_{i,k}^n}{\partial x} \right) + \frac{\partial}{\partial\sigma} \left(\frac{\nu_e}{h_i^n} \frac{\partial w_{i,k}^{n+1}}{\partial\sigma} \right) \end{aligned} \quad (9)$$

The equations (7)-(9) are solved for η efficiently by the conjugate gradient method. Similarly, Eqs. (5) and (6) are discretized and solved.

The continuity equation (1) can be used to derive an equation for non-hydrostatic pressure in real space as

$$\begin{aligned} a_P p'_P &= a_E p'_E + a_W p'_W + a_U p'_U + a_D p'_D \\ &+ a_{EU} p'_{EU} + a_{ED} p'_{ED} + a_{WU} p'_{WU} \\ &+ a_{WD} p'_{WD} + a_0 \end{aligned} \quad (10)$$

in which p' is the correction of the no-hydrostatic pressure. The coefficients such as a_P and the details are described by Stansby and Zhou (1998).

The σ mesh is refined near the bed and surface as in Stansby (1997).

Results

1. Wave over a plane bed

A wave over a plane bed is simulated. A mesh of 600x20 cells is used with $\delta x = 0.1\text{ m}$, $\delta t = 0.05\text{ s}$, and $h_0 = 1.0\text{ m}$. The period T is 4 s. The amplitude of uniform sinusoidal velocity at inflow is $U_0 = 0.2\text{ m/s}$. Fig. 1 shows velocity vectors at $t = 100\text{ s}$. Clearly, regular waves are propagating along the channel.

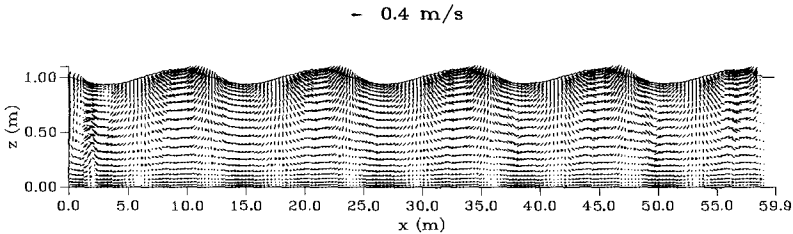


Figure 1: Wave over a plane bed

2. Wave over a bar with small side slope

The progressive wave considered here is the same as that studied experimentally by Beji et al. (1992). The wave flume is sketched in Fig. 2. The wave height is 2.0 cm and the period T is 2.0 s. A mesh of 320x21 cells is

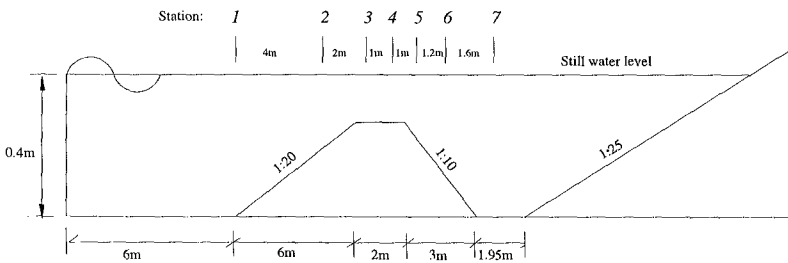


Figure 2: Sketch of the wave flume

used with $\delta x = 0.1\text{ m}$ and $\delta t = 0.005\text{ s}$. For the inflow boundary conditions, $U_0 = 0.09\text{ m/s}$ which generates a wave of 2.01 cm height and $h_0 = 0.4\text{ m}$.

Results after 17.5 s are shown in Figs. 3-5 with experimental data, showing good agreement. Results from the σ model without incorporating the moving grid are also plotted in Fig. 5. It is clear that the ALES model is superior to the σ model.

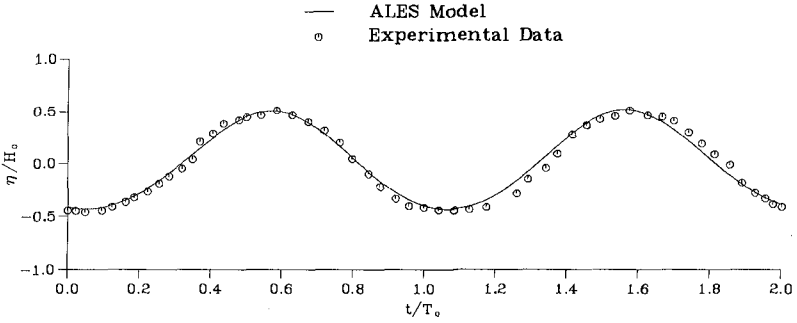


Figure 3: Comparison between model and experiment of the wave profile at station 1

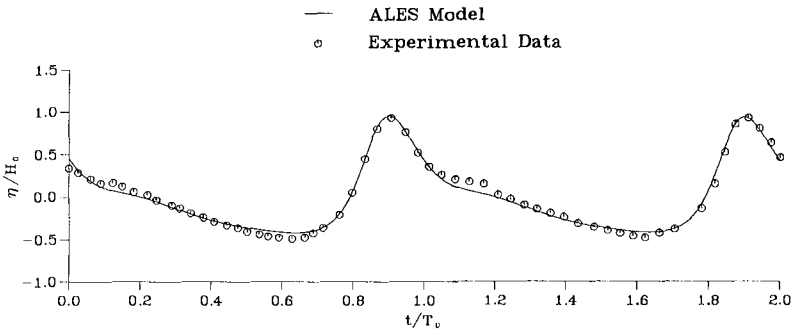


Figure 4: Comparison between model and experiment of the wave profile at station 3

3. Wave over a bar with steep side slope

Here a progressive wave over a bar with steep slope is considered. The flume is the same as that in the experiment by Ohyama et al. (1995) and is sketched in Fig. 6. The wave height is 5.0 cm and the period T is 2.01 s. A mesh of 600x21 cells is used with $\delta x = 0.1$ m and $\delta t = 0.005$ s. $U_0 = 0.2$ m/s generates a wave of 5.006 cm height and $h_0 = 0.5$ m. Results are presented after 33 s.

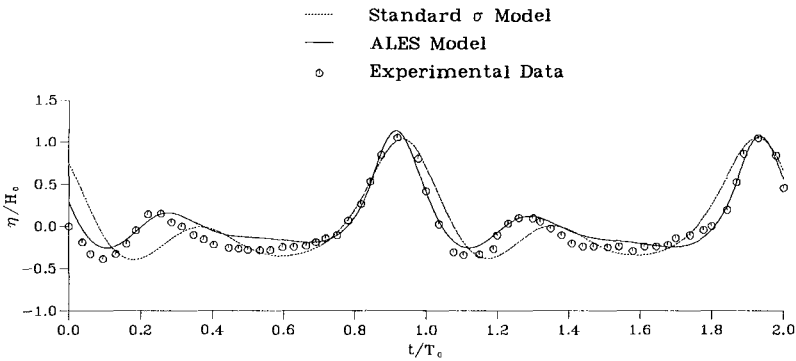


Figure 5: Comparison between model and experiment of the wave profile at station 5

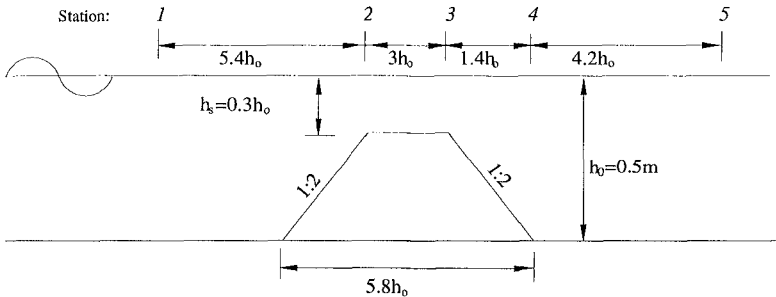


Figure 6: Sketch of experimental arrangement for wave over a bar with steep side slope

A comparison between experimental data and computations for station 3 is depicted in Fig. 7. The figure shows that the agreement is good. The results from the standard σ model are also plotted in the figure for comparison. Again, this shows that the ALES model is superior due to the incorporation of grid velocity

4. Comparison with hydrostatic model

In order to show the difference between the results predicted with and without non-hydrostatic pressure, a wave over a trench with the same geometry as described by Alfrink and van Rijn (1983) is simulated. A mesh of 170x20 cells is used in the numerical computation with $\delta x = 0.1 \text{ m}$, $\delta t = 0.01 \text{ s}$, $U_0 = 0.2 \text{ m/s}$ and $h_0 = 0.2 \text{ m}$. The period T is 3 s. Comparison of the surface

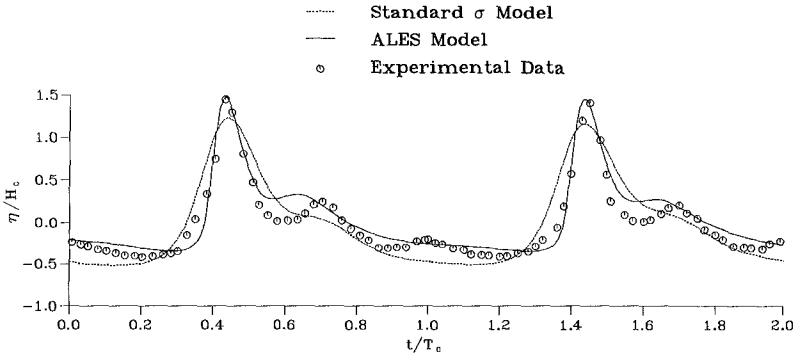


Figure 7: Comparison between model and experiment of the wave profile at station 3

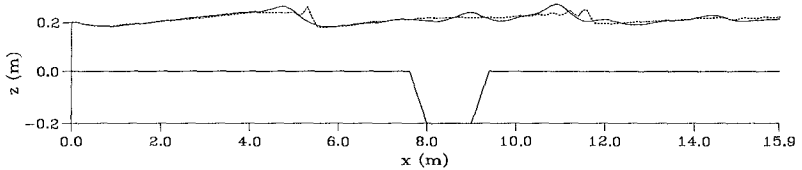


Figure 8: Comparison of surface profiles at $t = 20$ s with and without non-hydrostatic pressure: dashed line denotes the surface from hydrostatic pressure model

profiles is shown in Fig. 8.

5. A wave flow over a trench

A current over a trench has been investigated numerically and experimentally (Alfrink and van Rijn, 1983; Basara and Younis, 1995; Stansby and Zhou, 1998). No experimental studies of wave flow over a trench have been reported in the literature to our knowledge. However, this is an important problem in coastal engineering and is investigated numerically here. The trench used is the same as that investigated experimentally for a current (Alfrink and van Rijn, 1983) and is sketched in Fig. 9. A mesh of 170×30 cells is used in the numerical computation with $\delta x = 0.1$ m, $\delta t = 0.01$ s, $U_0 = 0.08$ m/s and $h_0 = 0.2$ m. The wave height is $h_w \approx 0.2h_0$ and the period T is 1 s. The streamlines are shown at $t = 20$ s in Fig. 10. The reflection coefficient is $K_r \approx 0.38$ and the transmission coefficient is $K_t \approx 0.44$, estimated after 4 wave crests have passed the trench. As comparison, a current over the trench

is shown in Fig. 11 (Stansby and Zhou, 1998).

6. A wave/current flow over a trench

Waves often occur in combination with a current. Here a wave/current flow over the same trench is simulated. To retain the same wave height, $U_0 = 0.2 \text{ m/s}$ and inflow boundary condition for velocity u is specified as

$$u_{in} = \frac{u_*}{\kappa} \log_e \left(\frac{30.0(z - z_0)}{k_s} \right) + U_0 \sin(2\pi t/T) \quad (11)$$

where $u_* = 0.033 \text{ m/s}$, $\kappa = 0.4$, $k_s = 0.002 \text{ m}$ and $z_0 = 0.00067 \text{ m}$. This gives wave height $H = 0.038 \text{ m}$ and mean current velocity $\bar{u} \approx 0.387 \text{ m/s}$.

Fig. 12 shows the streamlines at $t = 8.4 \text{ s}$. At this moment, there is clearly separation in the trench. There is also flow separation in the trench when $t = 8.7 \text{ s}$ as shown in Fig. 13. However, separation appears to disappear when $t = 8.9 \text{ s}$ as shown in Fig. 14. This highly unsteady separation is in contrast to the stable separation in a steady current (see Fig. 11) and attached flow in a wave alone.

Conclusions

In this paper, we present the application of the ALES model to wave flows. The results have shown that the ALES model is more accurate than the conventional shallow-water flow model in σ coordinate. When there is significant variation in either free surface or bed topography, the effect of the non-hydrostatic pressure on flows should not be ignored.

References

- Alfrink, B. J. and van Rijn, L. C. (1983). Two-equation turbulence model for flow in trench, *Journal of Hydraulic Engineering, ASCE* **109**(3): 941–958.
- Basara, B. and Younis, B. A. (1995). Predictions of turbulent flows in dredged trenches, *Journal of Hydraulic Research* **33**(6): 813–824.
- Beji, S., Ohyama, T., Battjes, J. A. and Nadaoka, K. (1992). Transformation of nonbreaking waves over a bar, *Coastal Engineering 1992, Proc. 23rd Int. Conf.*, Vol. 1, Venice, Italy, pp. 51–61.
- Hirt, C. W. (1970). An arbitrary lagrangian-eulerian computing technique, *Proc. 2nd Int. Conf. on Numerical Methods in Fluid Dynamics*, Berkeley, USA.
- Ohyama, T., Kioka, W. and Tada, A. (1995). Applicability of numerical models to nonlinear dispersive waves, *Coastal Eng.* **24**: 297–313.

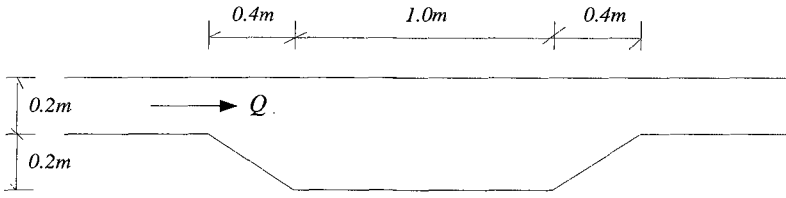


Figure 9: Sketch of the trench used in experiments (Alfrink and van Rijn, 1983)

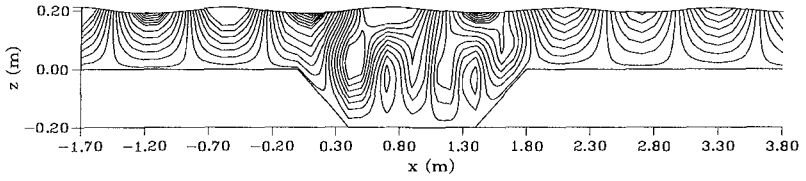


Figure 10: Streamlines for the wave over the trench $t = 20$ s

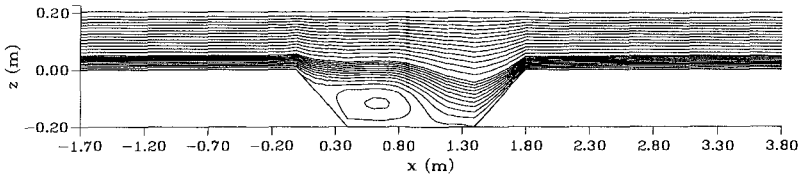


Figure 11: Streamlines for current flow over the trench (from Stansby and Zhou, 1998)

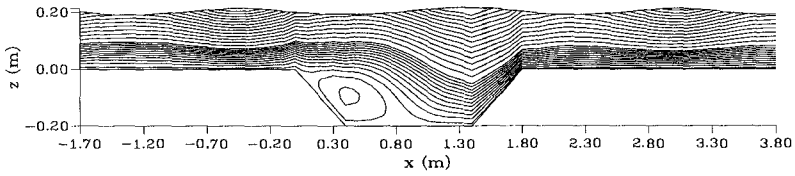


Figure 12: Streamlines for the wave/current flow over the trench: $t = 8.4$ s

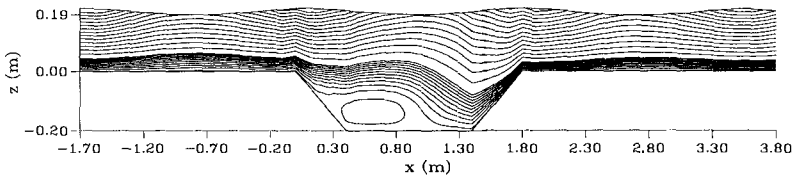


Figure 13: Streamlines for the wave/current flow over the trench: $t = 8.7$ s

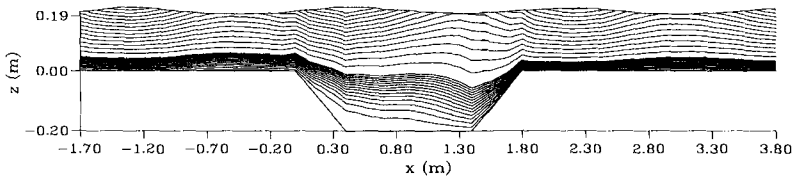


Figure 14: Streamlines for the wave/current flow over the trench: $t = 8.9$ s

- Rodi, W. (1993). *Turbulence models and their applications in hydraulics*, 3rd edn, IAHR.
- Stansby, P. K. (1997). Semi-implicit finite volume shallow-water flow and solute transport solver with $k - \epsilon$ turbulence model, *Int. J. Num. Meth. Fluids* **25**: 285-313.
- Stansby, P. K. and Zhou, J. G. (1998). Shallow-water flow solver with non-hydrostatic pressure: 2D vertical plane problems, *Int. J. Num. Meth. Fluids* **28**: 541-563.